Supplementary Information
Corn-Flowers-Like Transparent, Anti-moth Protein and Self-Cleaning Coatings for Vehicle Windshields

Wenjun Chan[a], Yimin Luo[b,c], Boran Hao[a], Zhongrun Qiu[a], Peiyan Yang[a], Haoyu Wang[a], and Zhuangzhu Luo*[a,c]*

a: School of Materials, Sun Yat-sen University, Shenzhen 518107, P. R. China

b: School of Materials and Energy, Foshan University, Foshan, 528000, PR China

c: Guangdong Engineering Technology Research Center for Tropical Marine Dynamic Anti-corrosion Materials, Sun Yat-Sen University, Shenzhen 518107, P. R. China

*E-mail: luoyimin1@fosu.edu.cn & luozhzhu@mail.sysu.edu.cn

Methods

Materials. Triethoxyvinylsilane (TEVS, 97%), Diethylene glycol (DEG, 99%), Hexadecane (98%) and 1H,1H,5H-perfluoropentyl-1,1,2,2-tetrafluoroethyl ether (HFO, 98%) were purchased from Macklin Co., Ltd. 2-(perfluorooctyl) ethyl methacrylate (FMA) (HDFDMA, 98%) and 2,2-Azobisisobutyronitrile (AIBN, Aladdin) were provided by Aladdin Bio-chem Technology Co., Ltd. (Shanghai, China). Liquid paraffin was purchased from Shandong Lierkang Medical Technology Co., Ltd. Olive oil, kerosene, hydraulic oil, and glycerol were obtained from Shenzhen Yinglida Lubricating Oil Co., Ltd. Methanol, ethanol, tetrahydrofuran(THF), ethyl acetate, dichloromethane, n-hexane, and hydrochloric acid were purchased from Xilong Scientific Co., Ltd., China. Glass substrates were acquired from Guangzhou Jiandaoshou Gene Technology Co., Ltd. PET films were purchased from Guangzhou Huiying Scientific Instruments Co., Ltd. Stamp pad ink, water-based ink, oil-based ink, fabrics, and sponges were all obtained from local stores. All chemicals were used as received without further purification.

Preparation of HBPSi. 0.16 mol of siloxane TEVS and 0.35 mol of DEG were added into a three-necked flask equipped with a mechanical stirrer, a nitrogen (N_2) inlet, and a thermometer. The mixture was slowly heated from 130 °C to 170 °C, followed by continuous stirring until no more distillate was generated. Theoretically, the distillate from the reaction should be low-boiling-point ethanol, which could be continuously separated from the reaction system via a condenser to drive the polymerization forward. The distillate was collected for Fourier transform infrared (FTIR) detection. Crude purification was performed via hexane solvent precipitation and reduced-pressure drying to remove small molecules and unreacted monomers from the reaction, ultimately yielding a liquid product.

Preparation of LHFO. LHFO was prepared via the copolymerization of HBPSi and FMA. The specific procedures are as follows, firstly, 0.33 g HBPSi was uniformly dispersed in 4 mL THF to form Solution A, separately, 0.004 g AIBN and 1.16 g FMA were weighed and dispersed in 12 mL HFO to form Solution B. Secondly, Solution A was added to a three-necked flask equipped with a constant pressure funnel and an N_2 inlet. The flask was then heated at 65 °C with magnetic stirring under N_2 protection, and Solution B was added dropwise into the flask within 2 h. After the completion of dropwise addition, the reaction was continued for 6 h, and a transparent coating solution was obtained after the flask was cooled to room temperature. The HFO and THF were removed by a rotary evaporator, and a milky white viscous LHFO was dissolved in an appropriate volume of ethyl acetate. The LHFO coating was prepared by a spray-coating strategy and thermal cured. The reaction procedures for other monomers and different ratios were consistent.

Preparation of Linear polymer SF. For comparison with hyperbranched fluorosilicone copolymers, linear polymer was synthesized through the commonly used free radical copolymerization reaction. For the preparation, 1 g TEVS, 1.5 g FMA, and 0.006 g AIBN were mixed in 10 mL THF, with the mixture allowed to react at 65 °C for 6 hours. SF coating was obtained using the same process.

Characterization. Proton nuclear magnetic resonance (^{1}H NMR) spectra were recorded on an AVANCE III HD 400 MHz spectrometer using DMSO-d_6 as the solvent. Fourier transform infrared (FTIR) spectroscopy was performed using a Bruker Invenio spectrometer over a wavenumber range of 4000–400 cm^{-1}. Experimental data were subjected to baseline correction and normalization. The transparency of the bare glass and LHFO coating were measured by a UV-6300 double beam spectrophotometer. The crystallinity of the samples was investigated using an X-ray diffractometer (Bruker D8 Advance) with Cu Kα radiation, scanning over a 2θ range of 5–60° and low-2θ region from 2.5° to 7.5°. Microstructures of the LHFO coatings and SF coating were observed by scanning electron microscopy (Tescan, Magna). The element distribution was performed via Energy-dispersive X-ray (EDX) spectrum imaging. Gel Permeation Chromatography (GPC, waters1525/waters 2414) was employed to determine the molecular weight distribution of HBPSi. X-ray photoelectron spectroscopy (XPS, ESCALAB Xi) were used to investigate the surface bonding properties of samples. (Fluorine contents on these surfaces were detected by XPS, which typically has an instrumental accuracy of ± 0.1%). MV3000 optical microscopy was employed to characterize the bending-induced creases of the coatings and the coverage of fingerprint fluid on the coating surfaces. Static contact angle (CA) and sliding angle (SA) were measured by a DSA-XROLL automatic contact angle meter. Water droplets, ethanol droplets and hexadecane droplets of 5 μL were used during contact angle measurements. Droplets volumes for sliding angle measurements were 10, 15 , 20 and 25 μL, respectively. The contact angle and sliding angle were obtained by measuring at least three different positions on each sample. The sliding velocities of water droplets, ethanol droplets and hexadecane droplets were measured by fixing a coated glass on a slope with varied inclination angles, and the entire sliding process of water droplets was monitored through a Canon EOS 80D camera. The captured data were processed and analyzed using software such as ImageJ and Origin. The sliding velocities were calculated according to the sliding distances measured and the sliding time. The high-speed camera with a frame rate of up to 2000 frames

per second (ACUPEVE 3.0, Optronis GmbH, Germany) was utilized to record the bouncing process of water droplets on the coating and the bouncing trajectories of the droplets were analyzed using PFV4 software.

Anti-adhesion test. Droplets with different surface tensions and viscosities (30 μL/40 μL) were separately allowed to slide down from bare glass and coated surfaces. The low viscosity of the coatings was evaluated by monitoring the sliding time of each droplet. In addition, high-viscosity glycerol was poured onto glass bottles coated with LHFO and uncoated glass bottles to verify the repellency of the coatings towards high-viscosity liquids.

Anti-graffiti test. Straight lines were separately drawn on each coating surface using brushes soaked with oil-based ink and water-based ink to evaluate the performance of each sample. Photographs were taken after the ink on the coating surface stopped shrinking.

Anti-fouling test. Approximately 0.2 mL of sludge water was dropped onto different glass coating surfaces. The samples were subsequently placed in a forced-air oven and dried at 40 °C for 3 hours. Each sample with dried sludge was slowly inclined to evaluate the performance of the coating.

Self-Cleaning test. Fine gravel was dispersed on glass surfaces and glass coating surfaces inclined at approximately 25°. Water was then dropped separately onto these different surfaces to observe the sliding behavior of the droplets on the surfaces.

Adhesive tape peeling test. A 3M adhesive tape was applied to the coating with a load of 0.5 kg for 30 s, and was peeled from the surface. This procedure was applied on coatings repeatedly and the SA of the slippery coating was investigated at a regular interval.

Water jet impacting test. The sample was placed in a container at an angle of 45°. A 500 mL plastic bottle was used to produce a high-speed water jet with a flow rate of approximately 1.5 L/min. The water jet was released at a vertical height of 35 cm from the coated glass, and the

slippery property of the coating was examined by testing the SA after every 1 L of water jet impact.

Flexibility test. Coated PET films were repeatedly bent 1000 times with a radius of curvature of approximately 1 cm, and the sliding angle (SA) of the smooth coatings was periodically measured. In addition, the coating was sprayed onto polyimide films, which were then bent with a radius of curvature of approximately 1 mm. After unfolding, a metallographic microscope was used to observe the damage of the coatings.

Tribological testing. An MS-T3001 tribometer (Lanzhou Huahui Instrument & Equipment Co., Ltd., China) was used to evaluate the tribological performance of the LHFO and SF coatings. A ball-on-disk configuration was adopted with a stainless steel ball (6 mm diameter) sliding against a disk of Φ 45 × 8 mm. Tests were conducted under unidirectional rotation (20 r min^{-1}) with a friction radius of 5 mm and a constant normal load of 2 N.

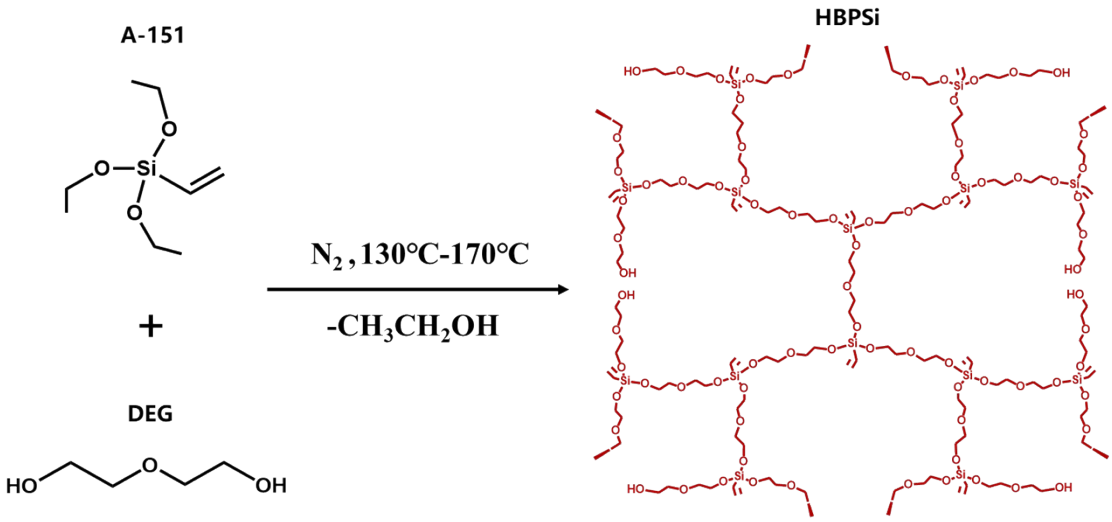

Scheme S1. Synthesis of HBPSi.

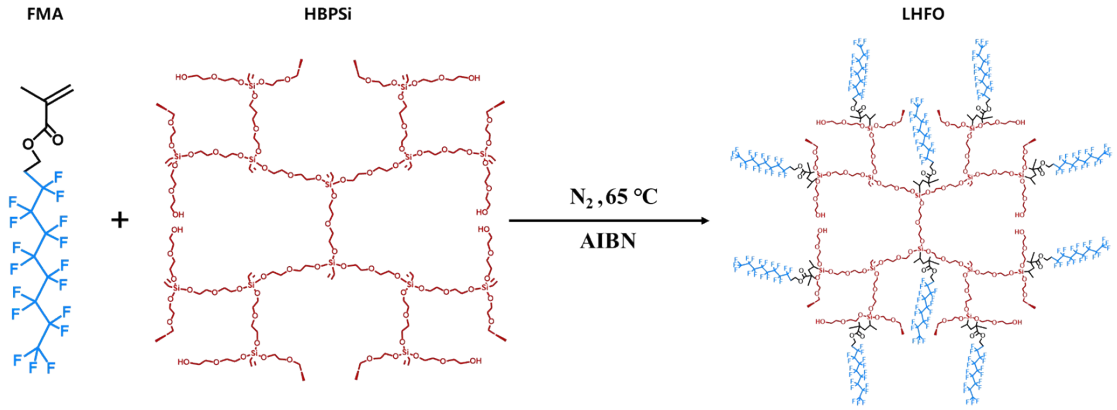

Scheme S2. Synthesis of LHFO.

Surface energy characterization.

The surface energy γ_{SV} of LHFOx and SF were measured via the Owen, Wendt, Rabel, and Kaeble (OWRK) method.[1] According to the OWRK model (**Equation S1**), surface energy γ is the sum of its polar component γ^p and dispersive component γ^d.

$$\gamma = \gamma^p + \gamma^d \qquad \text{(S1)}$$

Additionally, γ_{SL} (surface energy of the interface between liquid and solid) could be written as **Equation S2**:

$$\gamma_{SL} = \gamma_{SV} + \gamma_{LV} - 2\sqrt{\gamma_{SV}^d \gamma_{LV}^d} - 2\sqrt{\gamma_{SV}^P \gamma_{LV}^P} \qquad \text{(S2)}$$

Substituting equation S2 into Young's Equation yields **Equation S3**:

$$\frac{\gamma_{LV}\,(1+cos\theta)}{2\sqrt{\gamma_{LV}^d}} = \sqrt{\gamma_{SV}^p}\sqrt{\frac{\gamma_{LV}^P}{\gamma_{LV}^d}} + \sqrt{\gamma_{SV}^d} \qquad \text{(S3)}$$

Plotting $\frac{\gamma_{LV}\,(1+cos\theta)}{2\sqrt{\gamma_{LV}^d}}$ as a function of $\sqrt{\frac{\gamma_{LV}^P}{\gamma_{LV}^d}}$ yields a straight line, hence γ_{SV}^p and γ_{SV}^d can be calculated according to the slope and the intercept. The test liquids selected for this work are water (γ_{LV} = 72.80 mN m^{-1}, γ_{LV}^d = 21.80 mN m^{-1}, γ_{LV}^P= 51.00 mN m^{-1}) and hexadecane (γ_{LV} = 27.47 mN m^{-1}, γ_{LV}^d = 27.47 mN m^{-1}, γ_{LV}^P = 0.00 mN m^{-1}).

Supplementary Movies

Movie S1. Sliding process of a 10 μL hexadecane and paraffin oil droplet on the tilted LHFO-coating surface at an angle of 10° and 13°, respectively.

Movie S2. Under the same Reynolds number, water droplets fail to bounce on the bare glass and the SF-coated surface, whereas they can bounce on the LHFO-coated surface.

Movie S3. Water-based and oil-based ink trace left on bare glass and SF-coated while the LHFO-coated glass remained clean, showing remarkable anti-graffiti capability.

Movie S4. When water droplets are used to clean the sand particles spread on different surfaces, mud residues are left on the bare glass and the SF-coated surface, whereas the LHFO-coated surface remains clean.

Movie S5. Glycerol with ultra-high viscosity adheres to the entire inner wall of the glass bottle, whereas no glycerol residue is observed on the LHFO-coated glass bottle, demonstrating excellent anti-adhesion performance.

Movie S6. After water jet impact, water stains are left on the bare glass, whereas no traces are observed on the LHFO-coated surface.

Movie S7. Common contaminants in cycling environments are sprayed onto the windshield using a shower head spray bottle. A large amount of stains adhere to the uncoated areas, while the coated areas remaine clean.

Supplementary Discussion

FTIR spectroscopy serves as crucial evidence for confirming the successful synthesis of the target oligomer HBPSi. In the FTIR spectrum of DEG, the absorption peaks at 3458 cm^{-1} and 1123 cm^{-1} correspond to the stretching vibrations of hydroxyl groups (-OH) and ether linkages (C-O-C), respectively. The main absorption peaks of TEVS are located at 1600 cm^{-1} and 960 cm^{-1}, which can be attributed to the C=C bond and Si-O bond, respectively. In the FTIR spectrum of HBPSi, the absorption peaks at 3387 cm^{-1}, 2941 cm^{-1} & 2874 cm^{-1}, 1130 cm^{-1}, and 1081 cm^{-1} correspond to the stretching vibrations of hydroxyl groups (-OH), methylene groups ($-CH_2-$), C-O-C groups, and Si-O-C groups, respectively. The peak at 1610 cm^{-1}, which corresponds to the bending vibration of C=C bonds in HBPSi, is the most prominent absorption peak (Fig S1a). These absorption peaks confirm the successful synthesis of HBPSi. Distillate fractions were collected from the reaction system. The spectrum of the distillate obtained from the reaction is essentially identical to that of standard ethanol (Fig S1b). It can be basically confirmed that the distillate is ethanol, which serves as another important piece of evidence indicating the successful completion of the nucleophilic substitution polycondensation reaction. ^{1}H-NMR spectroscopy further confirms the structure of HBPSi. As shown in Fig S1c, in the spectrum of DEG (diethylene glycol), the proton peaks associated with hydroxyl groups (-OH) and methylene groups ($HO-CH_2-OH$) are labeled as 1&6 and 2&5, respectively, and can be observed at 4.57 and 3.51 ppm. The methylene groups adjacent to ether linkages (CH_2-O-CH_2) (labeled as 3&4) are observed in the signal peak at 3.40 ppm. In the spectrum of A-151, the proton peaks at 1.09–1.19 ppm are labeled as 1&5&7, those at 3.70–3.81 ppm as 2&6&8, those at 5.82–5.95 ppm as 3 and 3', and the proton peak at 6.07 ppm as 4. These proton peaks correspond to the $-CH_3$ groups in $Si-O-CH_2-CH_3$, the $-CH_2$ groups in $Si-O-CH_2-CH_3$, the two types of protons in $Si-CH=CH_2$ (i.e., the protons in $CH=CH_2$), and the protons adjacent to Si, respectively. In the spectrum of HBPSi, the proton peaks associated with primary carbons (in $Si-O-CH_2-CH_3$) and secondary carbons (in $Si-O-CH_2-CH_3$) correspond to H2 and H3,

respectively. The proton peaks associated with Si−CH=CH₂ are observed at 5.84–6.09 ppm, corresponding to H5 and H4/H4'. The methylene groups adjacent to ether linkages in DEG (CH₂-O-CH₂) appear at the position of H6, while the proton peaks of -OH and HO−CH₂−OH correspond to H7 and H8. Additionally, the proton peaks associated with secondary carbons (in Si−O−CH₂-) are observed at 3.59–3.64 ppm, corresponding to H1. These results strongly confirm the successful synthesis of the target oligomer HBPSi.

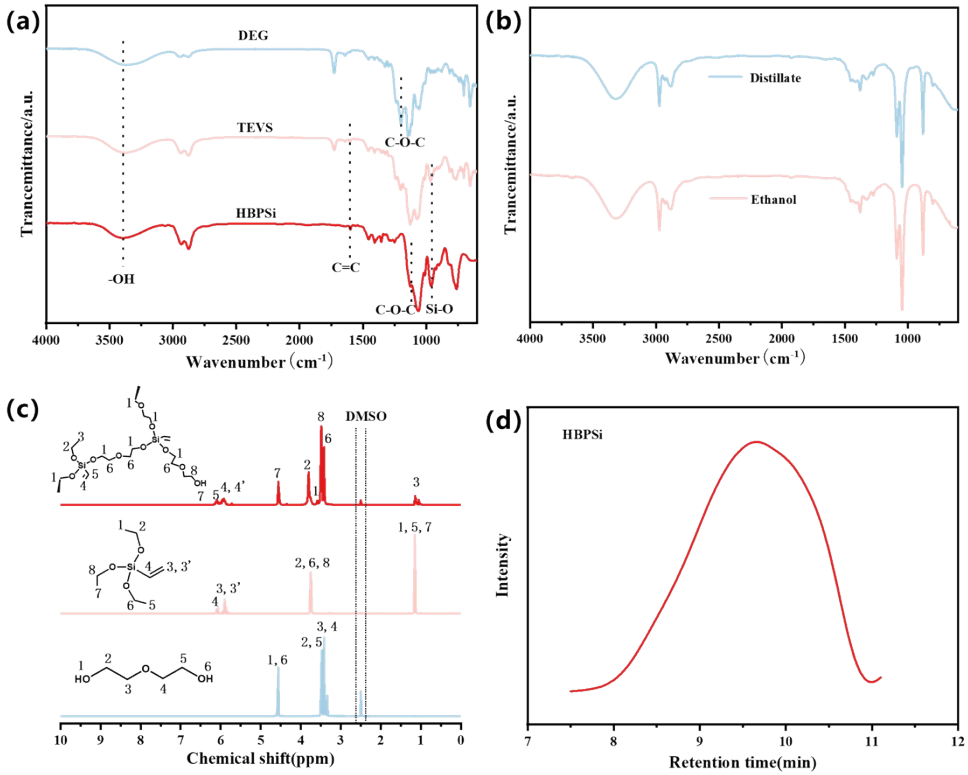

Fig. S1 Structural characterization of macromolecular oligomer HBPSi (a) FTIR spectra of HBPSi and reaction distillate. (b) FTIR spectra of distillate and standard ethanol. (c) The 1H NMR spectra of DEG, TEVS, and HBPSi with assigned protons. (d) GPC curve of HBPSi in THF.

FTIR spectra of the LHFO polymer before curing and the cured LHFO coating on glass were compared to examine structural changes during thermal curing (Fig. S2a). After curing, the

broad absorption band around ~3387 cm^{-1}, assigned to hydroxyl stretching, becomes weaker, while the absorption around ~1064 cm^{-1} associated with siloxane structures becomes more pronounced. These changes suggest the consumption of hydroxyl groups and the development of siloxane structures during thermal curing. Owing to the overlap of these bands with vibrations from the fluorosilicone network and the glass substrate, the FTIR analysis is interpreted qualitatively to support the occurrence of curing-induced siloxane condensation. In addition, cross-sectional EDS mapping (Fig. S2b) shows a continuous coating/glass interfacial region without obvious delamination.

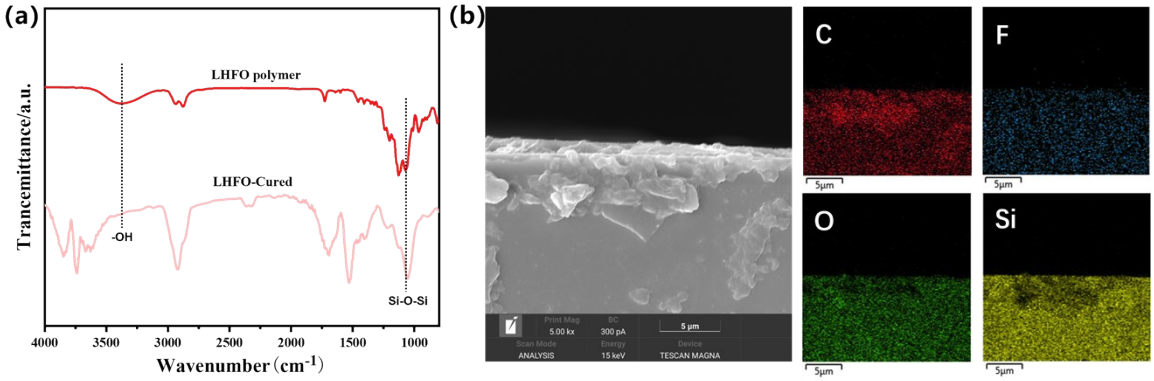

Fig. S2 Interfacial bonding analysis of the LHFO coating on glass. (a) FTIR spectra of the LHFO polymer before curing and the cured LHFO coating on glass. (b) Cross-sectional EDS mapping of carbon, fluorine, oxygen, and silicon across the LHFO/glass interface.

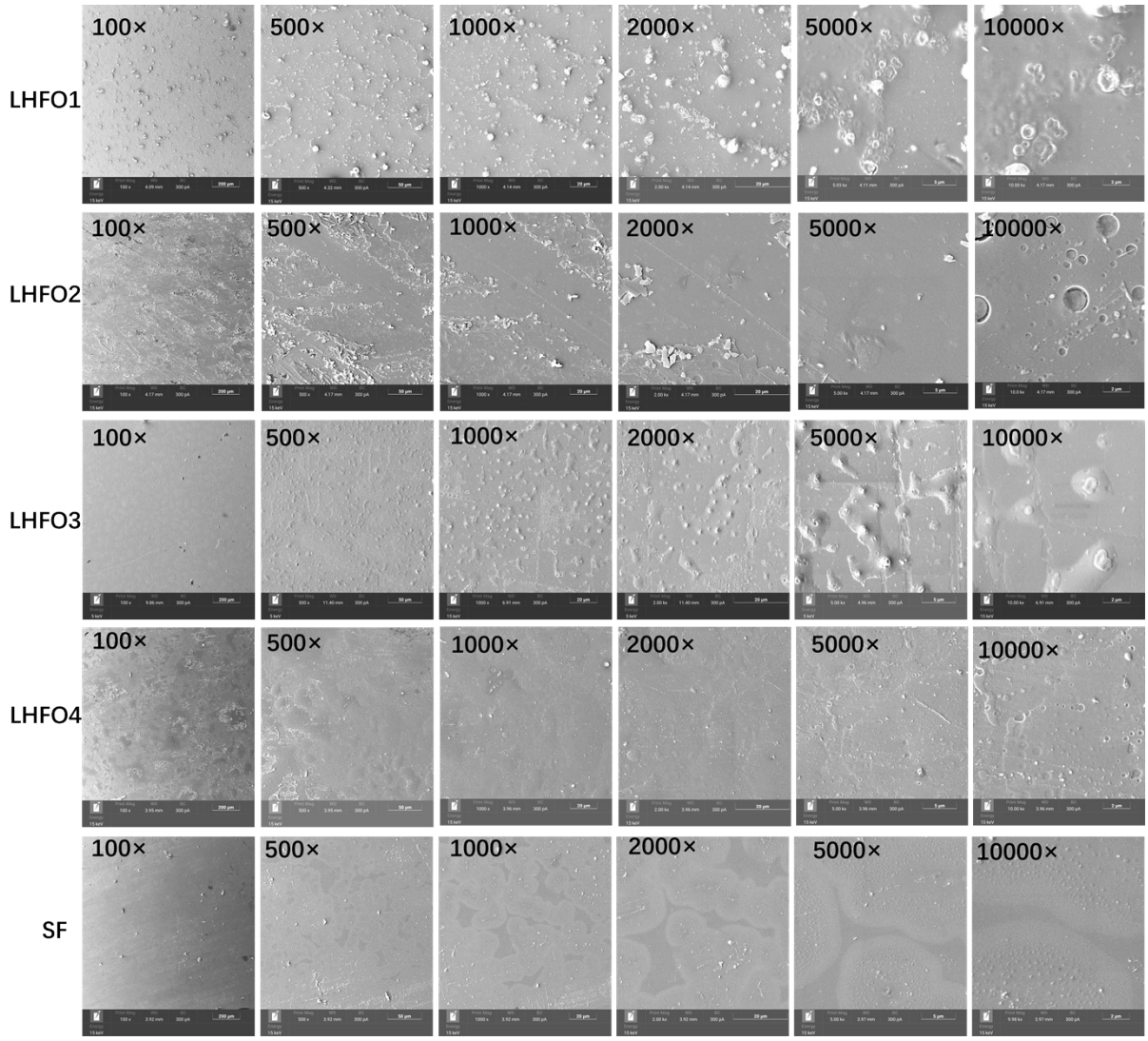

Fig. S3 SEM images of hyperbranched coatings and linear SF coatings.

From the SEM images and EDS of SF, it can be seen that the fluorine element signal does not show the characteristic enhancement of "surface aggregation". Due to the random entanglement between molecular chains, the migration of fluorine-containing functional groups to the surface is hindered, resulting in the failure of low-surface-energy functional groups to enrich on the surface.[2]

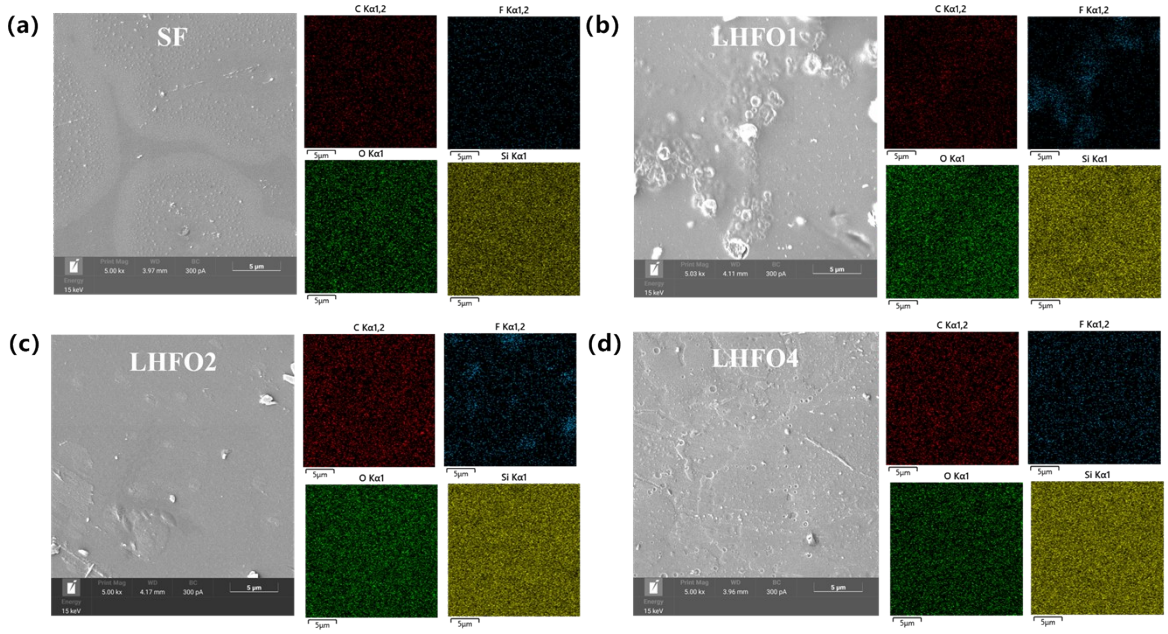

Fig. S4 SEM images and corresponding EDS elemental mappings of C, F, O, and Si. (a) SEM images and EDS mappings of SF. (b) SEM images and EDS mappings of LHFO1. (c) SEM images and EDS mappings of LHFO2. (d) SEM images and EDS mappings of LHFO4.

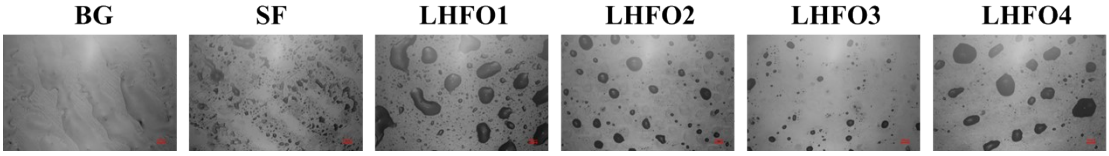

Fig. S5 Anti-fingerprint property of the LHFO coating.

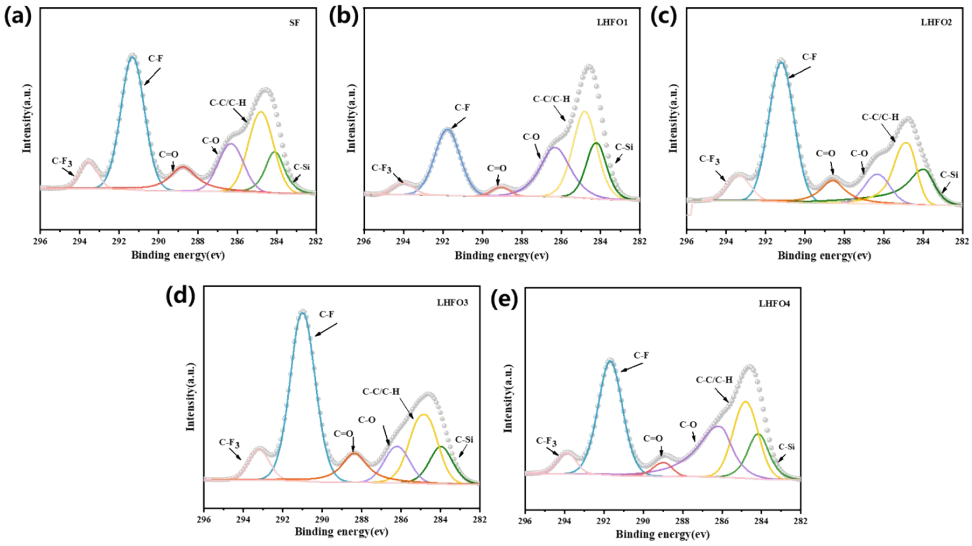

Fig. S6 XPS C1s spectra of LHFO and SF. (a) SF, (b) LHFO1, (c) LHFO2, (d) LHFO3, (e) LHFO4.

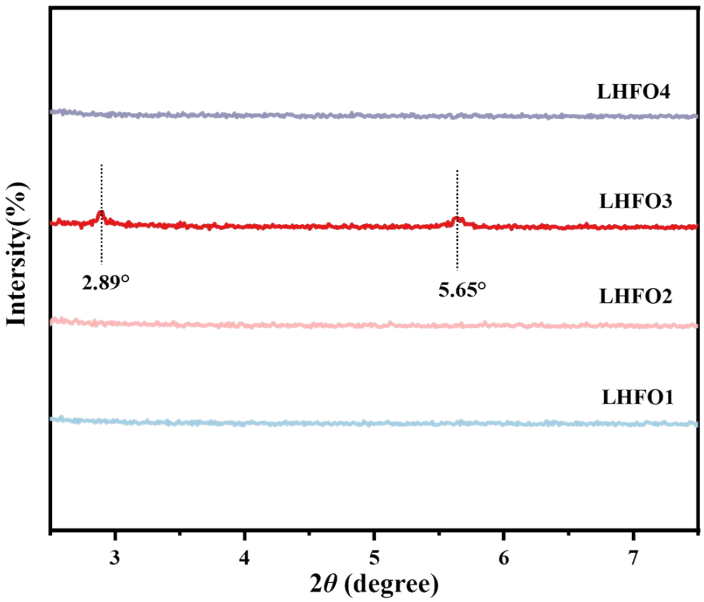

Fig. S7 XRD pattern of the LHFOx coatings in the low-2θ region from 2.5° to 7.5°, recorded using Cu Kα radiation (λ = 0.15418 nm).

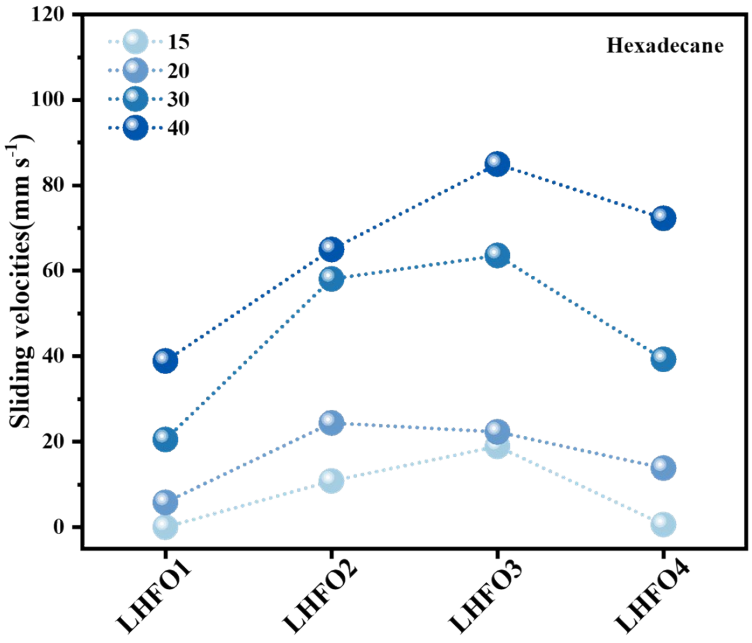

Fig. S8 Hexadecane-droplet sliding velocities on LHFOx-coated glasses at tilting angles of 15°, 20°, 30°, and 40°.

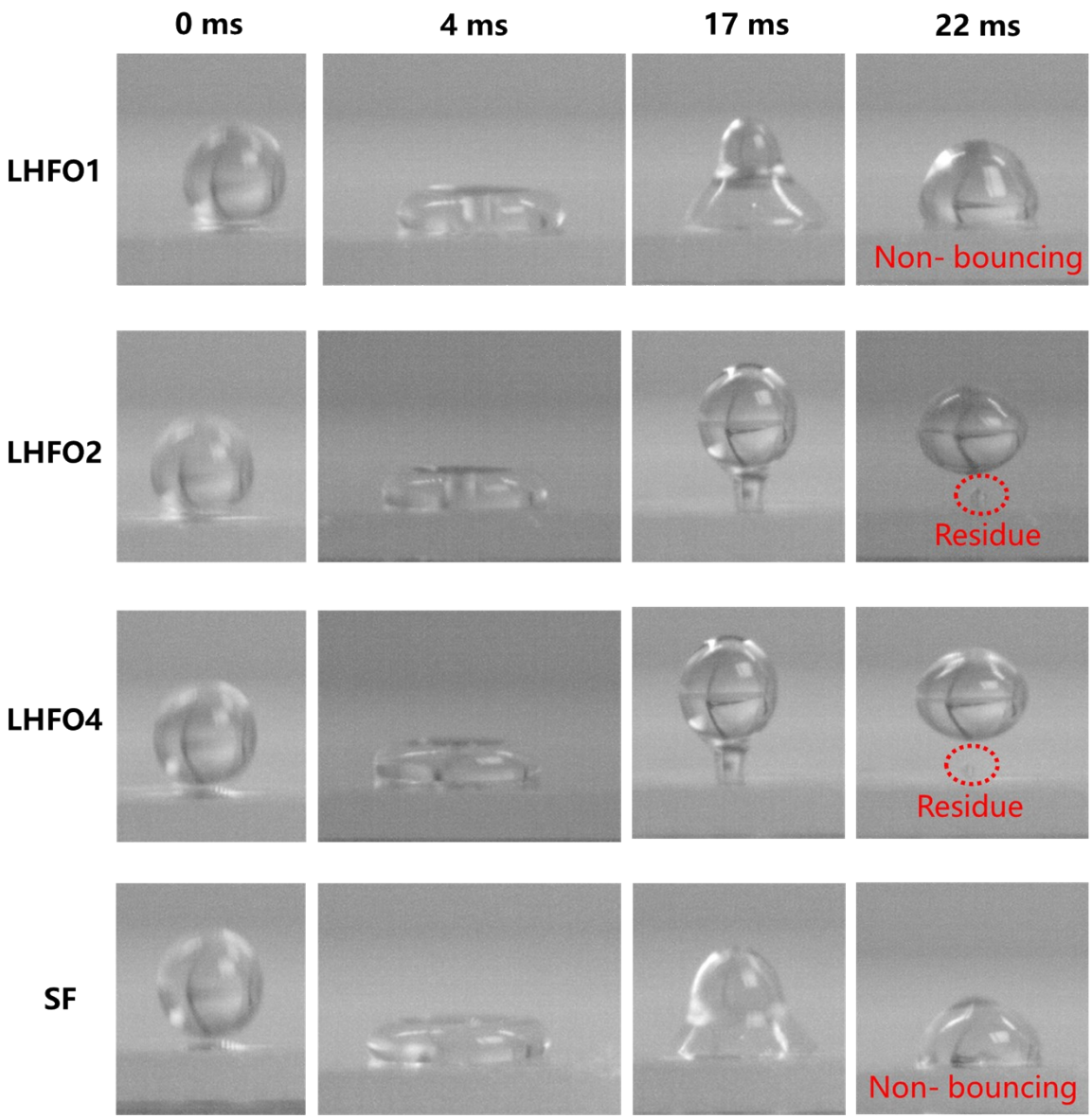

Fig. S9 Droplet bouncing snapshots of LHFO1, LHFO2, and LHFO3.

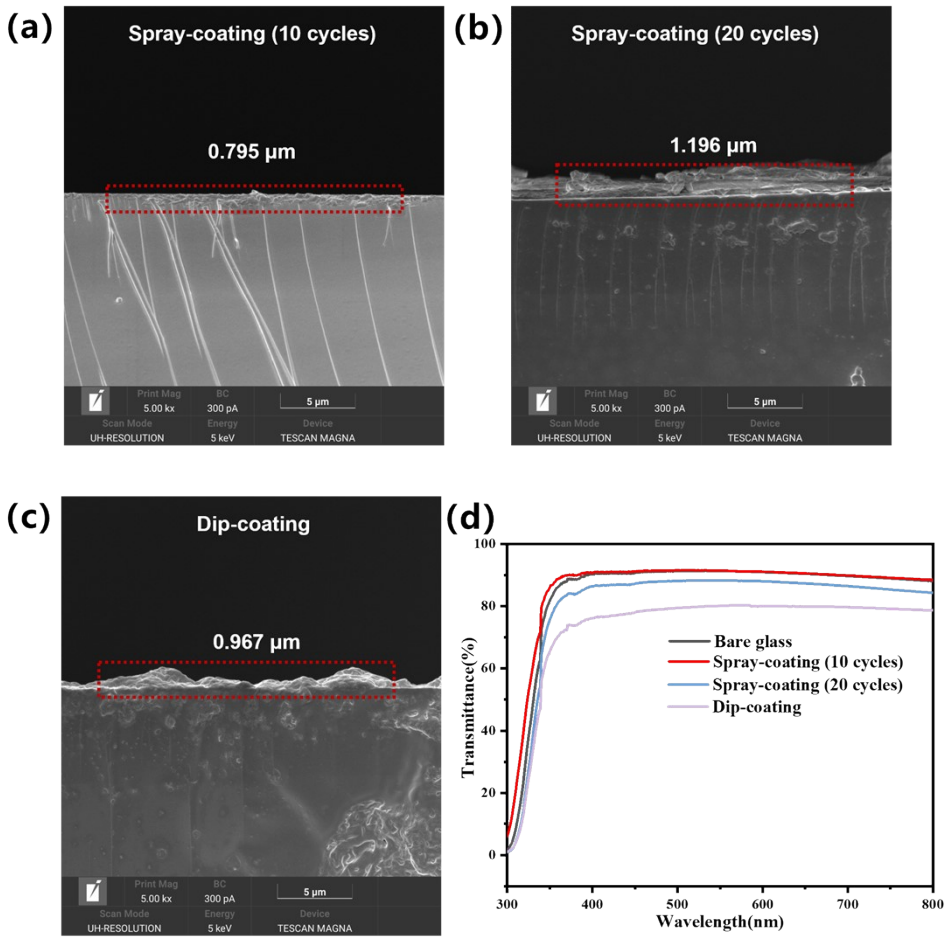

Fig. S10 Cross-sectional SEM images and optical transmittance spectra of LHFO coatings prepared under different deposition conditions. (a) Cross-sectional SEM image of the LHFO coating prepared by spray-coating for 10 cycles, showing a uniform and compact film with an average thickness of 0.795 μm. (b) Cross-sectional SEM image of the LHFO coating prepared by spray-coating for 20 cycles, showing an increased thickness of 1.196 μm. (c) Cross-sectional SEM image of the LHFO coating prepared by dip-coating, showing a thickness of 0.967 μm. (d) UV–vis transmittance spectra of bare glass and LHFO coatings prepared by spray-coating (10 cycles), spray-coating (20 cycles), and dip-coating. Scale bars in (a–c): 5 μm.

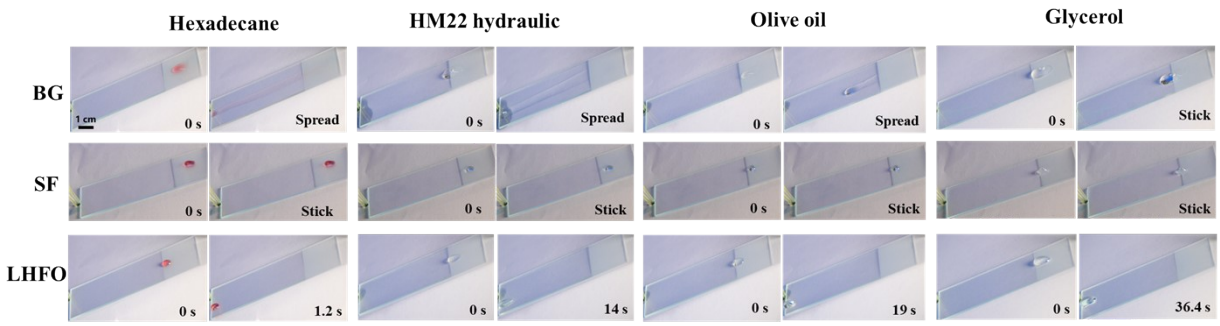

Fig. S11 Anti-fouling properties of the LHFO coating against oily liquids with different viscosities. Comparison of the behaviors of liquids on tilted bare glass (BG), linear SF-coated glass, and LHFO3-coated glass: hexadecane (15 μL), HM22 (15 μL), olive oil (15 μL), and glycerol (30 μL). Scale bar = 1 cm.

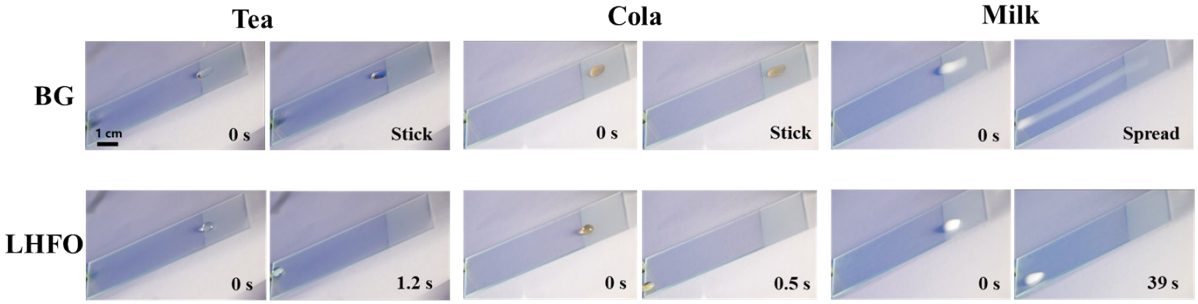

Fig. S12 Anti-fouling properties of the LHFO coating against different beverages. Comparison of the behaviors of liquids on tilted bare glass (BG) and LHFO3-coated glass: tea (30 μL), cola (30 μL), and milk (30 μL). Scale bar = 1 cm.

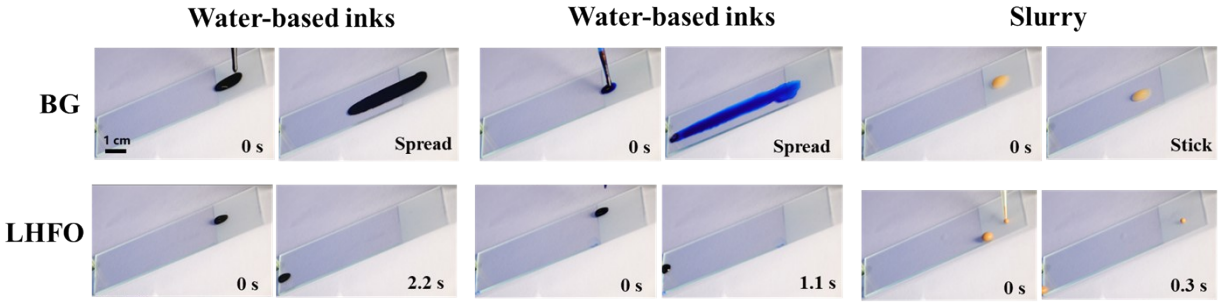

Fig. S13 Anti-fouling properties of the LHFO coating against other contaminants. Comparison of the behaviors of liquids on tilted bare glass (BG) and LHFO3-coated glass: water-based ink (30 μL), oil-based ink (30 μL), and sludge water (30 μL).

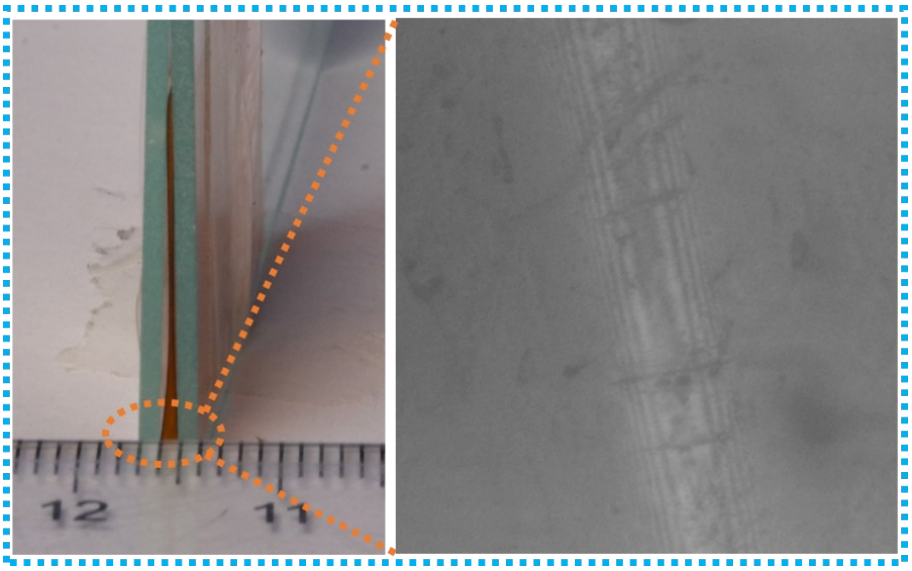

Fig. S14 Schematic diagram of the LHFO coating under bending (curvature <1 mm).

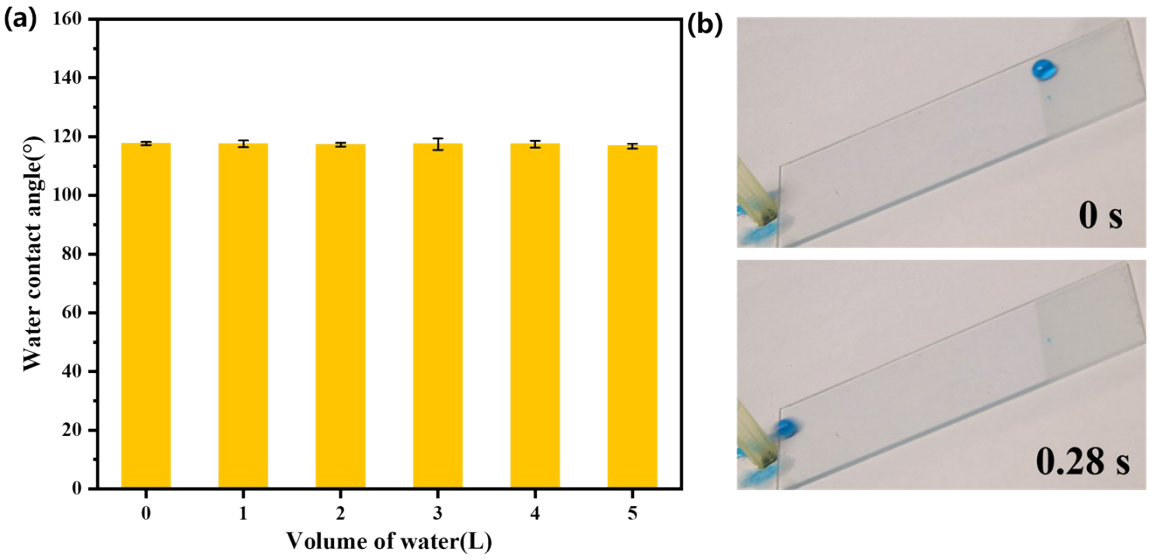

Fig. S15 Wettability and slidability of the LHFO coating under water flow impact. (a) change in water contact angle; (b) water droplet sliding diagram.

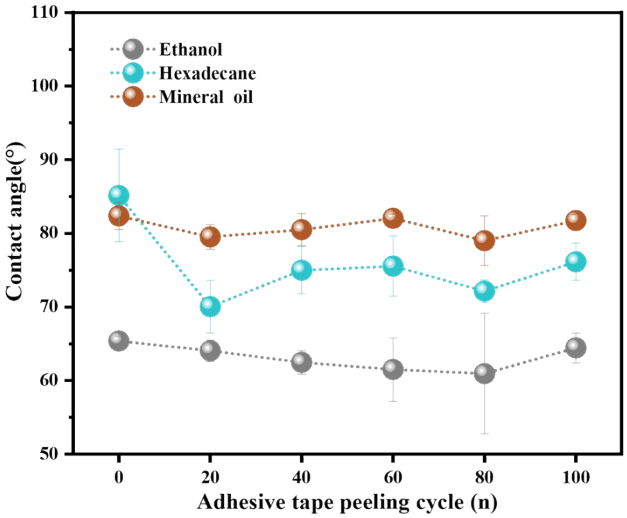

Fig. S16 Change in contact angle of the LHFO coating after 100 tape peeling cycles (test liquids: ethanol, hexadecane, and paraffin oil).

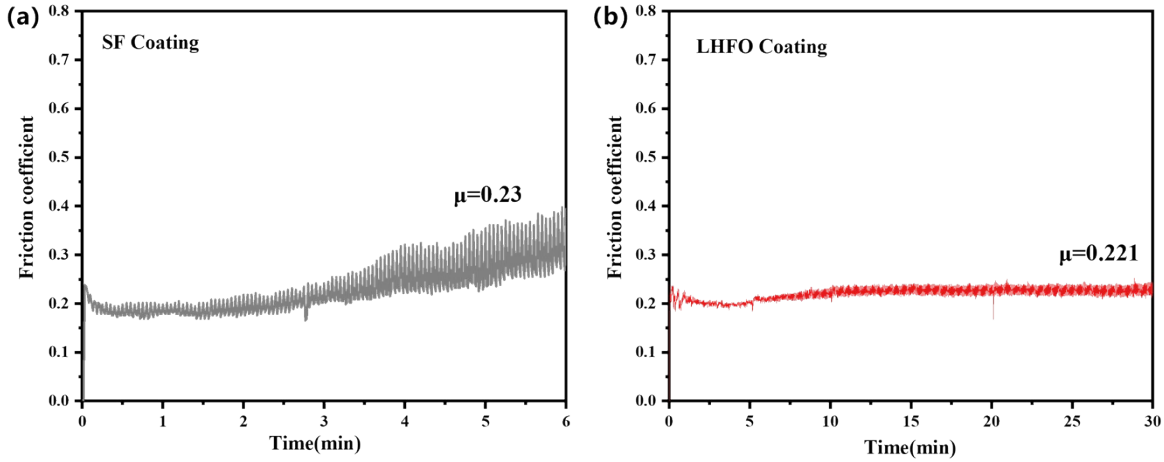

Fig. S17 Friction coefficient curves of SF and LHFO. (a) Friction coefficient curve of the SF coating. (b) Friction coefficient curve of the LHFO coating.

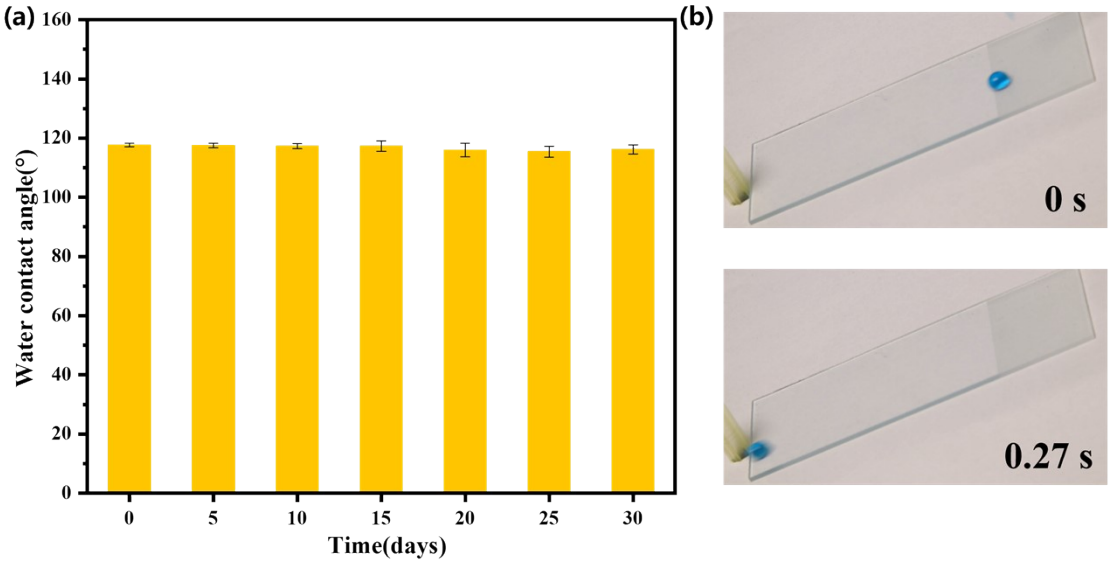

Fig. S18 Wettability and slidability of the LHFO coating at low temperature (-20 °C). (a) change in water contact angle; (b) water droplet sliding diagram.

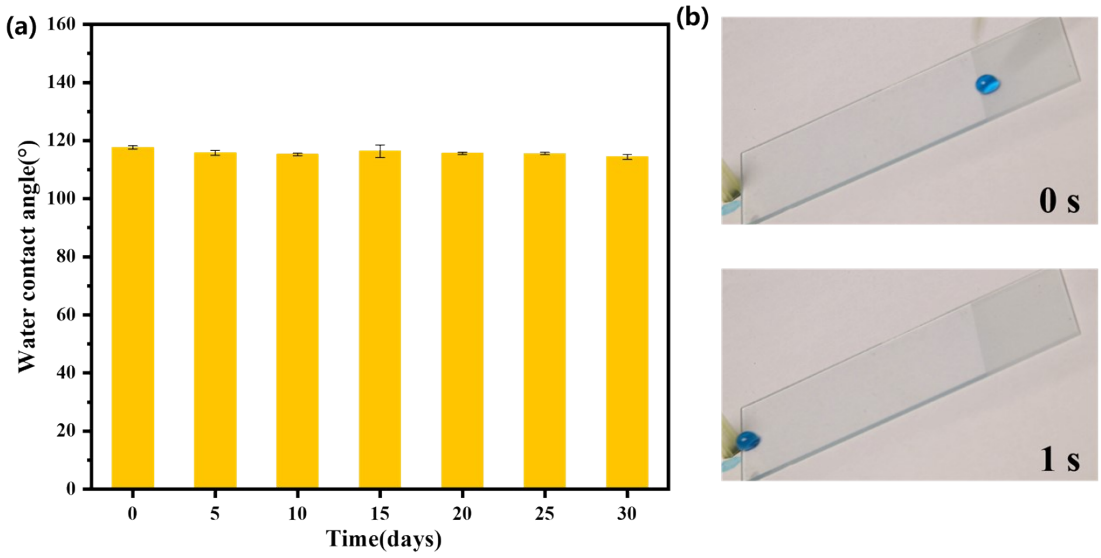

Fig. S19 Wettability and slidability of the LHFO coating under UV irradiation. (a) change in water contact angle; (b) water droplet sliding diagram.

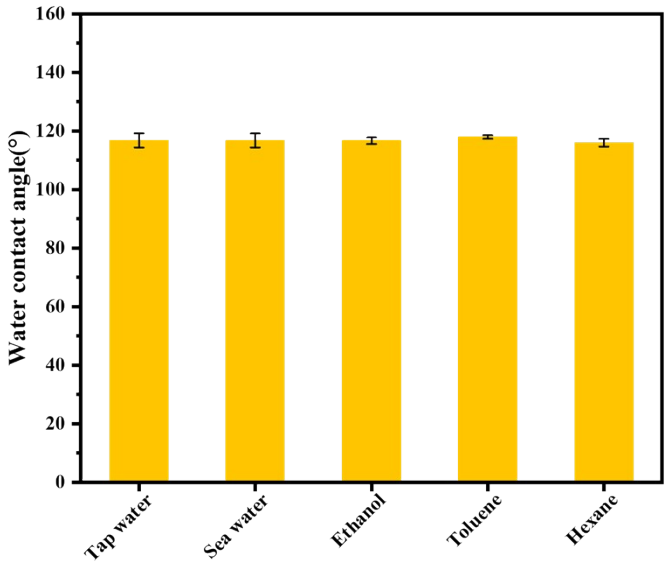

Fig. S20 Water contact angle of the LHFO coating after immersion in different solutions.

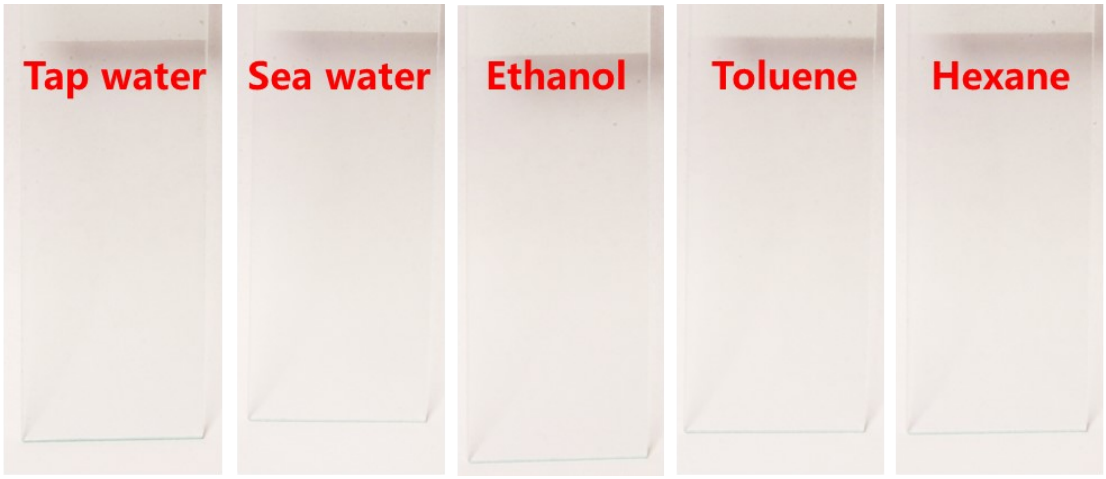

Fig. S21 Photographs of the LHFO coating after 24 h of immersion (no residual liquid droplets observed).

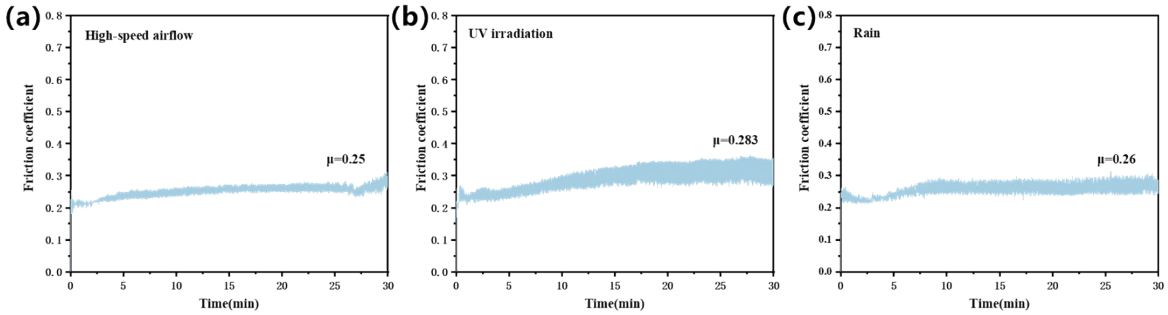

Fig. S22 Friction coefficient curves of LHFO after high-speed airflow, UV irradiation, and water immersion. (a) Friction coefficient curve of LHFO after high-speed airflow treatment. (b) Friction coefficient curve of LHFO after UV irradiation. (c) Friction coefficient curve of LHFO after rain water immersion.

Fig S18a displays the FTIR spectra of bird dropping and insect protein, the N-H stretching vibration appears around 3380 cm^{-1}, a signature of amino/amide moieties in pancreatin. The C-H stretching vibration at ~2920 cm^{-1} (from hydrocarbon segments of its amino acid residues), and at ~1650 cm^{-1}, absorptions attributed to C=O stretching and C-N/N-H (e.g., amide bond) vibrations are detected, with these signals (particularly the C=O absorption) being markedly stronger in bird droppings. The FTIR spectrum of paraffin oil (Fig S18b) presents that its characteristic peaks are dominated by vibrations of the $-CH_3$ group at 2960 cm^{-1} and 1461 cm^{-1}, which are consistent with the typical infrared spectral features of alkane-based paraffin oil.

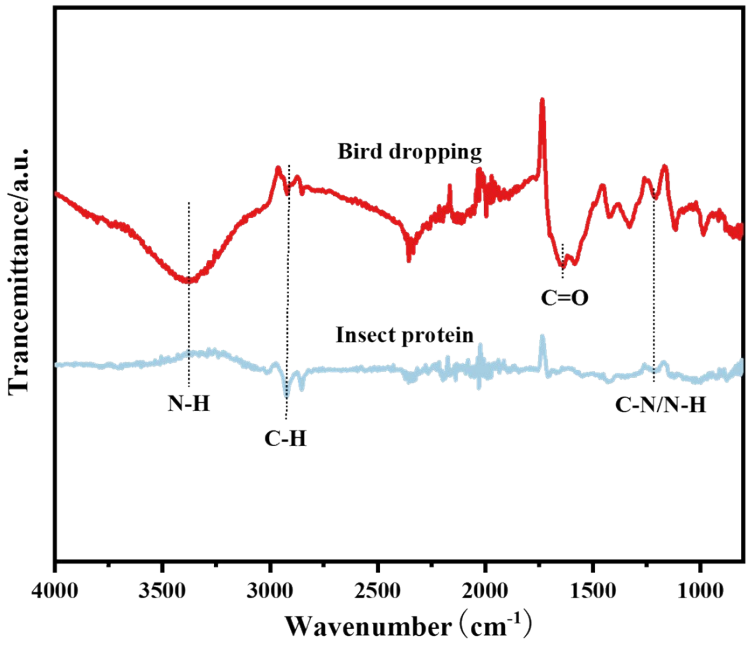

Fig. S23 FTIR spectra of bird dropping and insect protein.

Supplementary Tables

Table S1. Molar ratios of FMA and HBPSi, as well as the surface fluorine content and surface energy of the LHFO coating.

Sample	n_{FMA} / n_{HBPSi}	Fluorine contencts (%)	Surface energy (mN/m)
LHFO1	~15/1	52.77	15.07
LHFO2	~20/1	75.01	10.89
LHFO3	~25/1	78.36	8.89
LHFO4	~30/1	66.74	12.95

Table S2. Comparative wettability and mechanical properties of LHFO, HBPSi, and SF coatings.

Coatings	CA (water/oil)	SA (water/oil)	Bending radius	Adhesion rating
LHFO	118°/85°	15°/6°	<1 mm	5B
HBPSi	94°/23°	not sliding	1 mm	4B
SF	111°/75°	57°/20°	>1 mm	4B

Table S3. Comparison of remarkable performance of LHFO coating with prior literature.

Structure/Type	**Substrates**	**Relative transmittance**	**CA(°)/SA(°)**	**Repellency limits/ Surface tension of coating**	**Muti-functionality**	**Durability**	**Ref.**
8-MAPOSS/ Transparent self-cleaning coating	Glass, Steel.	T_{avg}: 90.5% (T_{glass}: 87.2%)	5/20 μL Water: 118/>25 Oil: 88/>25	Asphalt sliding/ 9.39 $mN \cdot m^{-1}$	Self-cleaning: Performed. Anti-adhesion: asphalt.	UV exposure test: 6 days. Chemical stability test: NaCl, ethanol, HCl (pH=1), and NaOH (pH =12). Thermal stability test: asphalt sliding through the coated pipe at 160 °C and ethanol droplets on coated stainless-steel sheet at -70 °C.	3
POSS-$(SH)_8$/ Liquid-like Surface	Glass, PET, Aluminum.	T_{avg}: ~88% (T_{glass}: 87%)	5/15 μL Water: >20 (SA) Oil: <15 (SA) Ethanol: ~30/~6	Crude-oil droplet sliding/ 22.5 $mN \cdot m^{-1}$	Anti-adhesion: anti-crude oil. Anti-fouling: anti-bacteria, anti-protein.	Adhesive tape peeling test: 1000 cycles. Flexibility test: 1000 cycles. Chemical stability test: 24 h in n-hexane, dichloromethane, toluene, and ethanol.	4
FGMPOSS/ Liquid-like coating	Glass, PET.	T_{avg}: 95%	5/15 μL Water:117/35	11.8 mN m^{-1}	Self-cleaning: Performed. Anti-graffiti: Performed.	Abrasion test: Steel wool, 300 cycles.	5
Ladder-like/ Polysilsesquioxanes coating	Si wafers, PETG, PMMA.	No Performed	2 μL Only water:87	No Performed	Anti-fouling: anti-bacteria.	Chemical stability test: the coatings in 1× PBS for 9 days.	6
Ladder-like polysilsesquioxane/ Liquid-like coating	Glass, PET.	T_{avg}: 99%	5/15 μL Water:114/32 Diiodometha: 94/12 Hexadecane: 68/27	12.3 mN m^{-1}	Self-cleaning: Performed Anti-graffiti: Performed	Abrasion test: Steel wool, 300 cycles.	7
Ladder-like/ "Liquid-Like" omniphobic solid anti-biofouling coating	Glass, PDMS, Steel, Aluminum.	T_{avg}: >90%	15 μL for SA. Water: ~18 Diiodometha: ~9 Hexadecane: ~10 Ethanol: ~12	15 μL Water and ethanol across the LL-OSC at 18° and 12° tilting angles.	Anti-graffiti: Performed Anti-fouling: anti-bacteria, anti-protein.	Flexibility test: 1000 cycles, bending curvature<1 mm. Water jet impacting test:1.4 L min^{-1}). Adhesive tape peeling test: 100 cycles. Thermal stability test: 100°C and UV exposure for 30 days. Chemical stability test: exposure to pH 1, pH 12, SDS, CTAB, artificial	8

						seawater for 48 h. DI water stability for 30 days	
V4D4 polysiloxane backbones /Lubricant-infused stretchable coating	PVA, Hydrogel, Filter paper, Wafer, PDMS, Ecoflex, PVC, PP, Aluminum alloy.	Non-transparent	10/10 μL Only water: 120/8	High liquid repellency for FBS, DMSO, blood, EG, and DIW.	Anti-fouling: plasma proteins and biofilm-forming bacteria.	Flexibility test: repeated cyclic stretching > 2000 cycles at 150% strain. Chemical stability test: high biocompatibility.	9
V4D4/ Fluorine-free amphiphilic copolymer	Glass, Aluminum, Si wafers	No Performed	Water hysteresis of 17°	The coating reduces Pseudomonas aeruginosa attachment by over 90%, *Cellulophaga lytica biofilm* by 55%, *Navicula incerta* by 99.7%.	Anti-fouling: Pseudomonas aeruginosa, *Cellulophaga lytica biofilm, Navicula incerta.*	Chemical stability test: in H_2SO_4 or NaOH for 5 h. Incubation in 1×PBS for 9 days.	10
V4D4/ Cyclotetrasiloxane-based Hybrid Superhydrophobic Fabrics	Fabric	No Performed	Only water: 150	low surface energy and roughness.	Self-cleaning: Performed. Anti-fouling: separate a range of oil/water mixtures.	Chemical stability: salt solutions and aqueous solutions of different pH values for 24 h.	11
perfluoropolyether chains polymer brush/ Hybrid omniphobic surface	Glass	T_{avg}: 98% (T_{glass}: 98%)	5 μL/20 μL Water: ~108/~20 silicon oil SA: ~50	High viscosity silicon oil can slide with a 50° sliding angle/ 9.8 mN·m^{-1}	Self-cleaning: Performed. Anti-graffiti: Performed.	Mechanical stability: Wettability of is nearly invariable after 200,000 friction cycles under a 100 kPa pressure.	12
Polymer brush / Liquid-repellent anti-smudge hybrid coating	Glass	T_{avg}: 93.3% (T_{glass}: 90.3%)	4 and 9 μL for CA,30 and 10 μL for SA. Water: 96/4.5 Hexadecane: 30/3	n-hexadecane repellency	Self-cleaning: Performed. Anti-graffiti: Performed. Anti-adhesion: bacterial anti-adhesion.	Long-term stability: 7 months Chemical stability: Resistance to ethanol.	13
Other Structure/ Solid-like slippery coating	Glass, Aluminum	T_{avg}: 80.6% (T_{glass}: 90.0%)	5 μL Water-based liquid: 100/2.5	liquid glue with a super - high viscosity of ≈1200 mPa·s can slide off.	Self-cleaning: Performed Anti-adhesion: non-sticking ability to the self-adhesive advertising paper.	Water jet impacting test: 1.1 L. UV exposure test: 30 days. Thermal stability test: 20°C to 240°C, 10 min Chemical stability test: no slippery capability for organic solvents.	14
Other Structure/ Bioinspired Cellulose-Based Ultra-Slippery Film	Glass, Solar panels	T_{avg}: >87% (T_{glass}: 95.0%)	Water: 118/0.4	resist the accumulations of dust, mud, bird droppings, and algae.	Self-cleaning: Performed Anti-fouling: sludge, bird droppings. Anti-adhesion: low ice adhesion strength.	Thermal stability test: stored in air for 6 months. Stable at 120 °C. Adhesive strength (9.5 MPa) only decreased to 9.3 MPa after 30 temperature cycles.	15
Hyperbranched/ transparent, anti-moth protein and self-cleaning coatings	Glass, PET, Polyimide film, Plastic, Sponge, Fabric, PMMA, Si wafers.	T_{avg}: 91.8% (T_{glass}: 91.1%)	5/15 μL Water: 118/15 Ethanol: 65/10 Hexadecane: 85/6 Paraffin: 83/5	10 μL droplet of hexadecane or paraffin oil can slid with an inclination angle of only 10°-13°. Repel high viscosity glycerol (~1412 mPa·s). For 5 μL water droplet with a Weber number of 10.7, it can bounce once on LHFO surface./	Self-cleaning: Performed. Anti-graffiti: Performed. Anti-fingerprints: Performed. Anti-fouling: sludge, bird droppings, insect protein. Anti-adhesion: low attachment for glycerol (1412 mP·s) and hexane (18.4 mN·m^{-1}).	Flexibility test: 1000 cycles, bending curvature<1 mm. Water jet impacting test: 5 L, 1.5 L/min. Adhesive tape peeling test: 100 cycles. Thermal stability test: –20°C, 30 days and 100°C, 7 days. UV exposure test: 30 days. Chemical stability test: 24 h in various organic solvents (e.g., ethanol, toluene, hexane, etc.)	**This work**

				8.89 $mN \cdot m^{-1}$			

Table S4. Thickness-dependent performance comparison of LHFO coatings prepared under different deposition conditions.

Preparation method	Thickness (μm)	WCA (°)	OCA (°)	Transparency (%)
Spray-coating (10 cycles)	0.795	115	75	91.5
Spray-coating (20 cycles)	1.196	110°	74°	88.3
Dip-coating	0.967	86°	32°	80.1

Table S5. The surface tension and viscosity coefficients for all test liquids.

Liquids	Surface tension (mN/m）	Viscosity coefficients (mPa·s）	Liquids	Surface tension (mN/m)	Viscosity coefficients (mPa·s)
Water	72.8	1.002	Glycerol	63.4	1412
Toluene	28.5	0.56	Olive oil	36	84
Hexadecane	27.5	3.34	Paraffin oil	26	30
Ethanol	22	1.2	Hydraulic oil	22 Cst	19.14
Hexane	18.4	0.31	Kerosene	28	2.5

References

[1] a) D. H. Kaelble, J. Adhes. 1970, 2, 66; b) D. K. Owens, R. C. Wendt, J. Appl. Polym. Sci. 1969, **13**, 1741.

[2] S. Pan, A. K. Kato, J M Mabry, A. Tuteja, J. Am. Chem. Soc. 2013, **135**, 578-581.

[3] L. Liu, M. Zhang, Y. Yan, Y. Zhou, S. Wang, P. Pi, X. Wen, Y. Qian, L. Jiang, *Chem. Eng. J*. 2024, **482**, 148921.

[4] W. Zheng, J. Huang, X. Zang, X. Xu, W. Cai, Z. Lin, Y. Lai, *Adv. Mater*. 2022, **34**, 2204581.

[5] D.N. Bender, G. Liu, *Chem. Eng. J*. 2023, **464**, 142702.

[6] S. Park, J.-Y. Kim, W. Choi, M.-J. Lee, J. Heo, D. Choi, S. Jung, J. Kwon, S.-H. Choi, J. Hong, *Chem. Eng. J*. 2020, **393**, 124686.

[7] Z. Lai, G. Liu, *ACS Appl. Mater. Interfaces* 2022, **14**, 35138–35147.

[8] A. Shome, I. Martinez, V.D. Pinon, J.C. Moses, M. Garren, A. Sapkota, N. Crutchfield, D.J. Francis, E.J. Brisbois, H. Handa, *Adv. Funct. Mater*. 2024, **34**, 2401387.

[9] T.Y. Kim, S. An, Y. Kim, S.Y. Han, J. Lee, K. Park, S. Kim, J. Park, S.A. Kim, J.J. Chung, S.-W. Cho, J. Seo, *Adv. Funct. Mater*. 2024, **34**, 2312740.

[10] H. Shu, A. Khlyustova, K.-W. Park, S. Stafslien, G. Kang, P. Chen, S. Shindler, R. Yang, *Adv. Funct. Mater*. 2025, 2502065.

[11] M.-S. Liu, R. Kunthom, B. Dudziec, H.-Z. Liu, *Chin. J. Polym. Sci*. 2025, **43**, 1022–1031.

[12] Z. Ma, Y. Wu, R. Xu, Z. Li, Y. Liu, J. Liu, M. Cai, W. Bu, F. Zhou, *ACS Appl. Mater. Interfaces* 2021, **13**, 14562–14568.

[13] Y. Wang, J. He, *J. Colloid Interface Sci*. 2021, **594**, 781–790.

[14] W. Pan, Q. Wang, J. Ma, W. Xu, J. Sun, X. Liu, J. Song, *Adv. Funct. Mater*. 2023, **33**, 2302311.

[15] H. Wang, C. Mo, X. Zhang, J. Zheng, G. Han, H. Qiu, B. Li, K. Yin, Z. Zhou, *Adv. Sci*. 2025, e14626.